GeoVirtual 2020 September 14-16 Resilience and Innovation

Terrestrial laser scanning (TLS) deformation monitoring of a high-fill embankment in the Arctic

Dylan Stafford, Earl Marvin De Guzman, Samuel Kaluzny, & Marolo Alfaro
University of Manitoba, Winnipeg, Manitoba, Canada
Lukas Arenson
BGC Engineering Inc., Vancouver, British Columbia, Canada
Guy Doré
Université Laval, Laval, Québec, Canada

ABSTRACT
The Inuvik-Tuktoyaktuk Highway (ITH) in Northwest Territories, Canada was built during winter on ice-rich continuous permafrost with no cuts in the ground to preserve the permafrost foundation. Several high-fill sections were required along the highway to meet vertical geometry specifications. Embankments in Arctic regions are susceptible to deformations due to thawing of the frozen fill material and permafrost foundation at the embankment toes. One high-fill section along ITH was reinforced with woven geotextiles to reduce slope movements. The reinforced section and an adjacent control section were instrumented to monitor slope movements. Terrestrial laser scanning (TLS) was conducted at the research site in August 2018 and June 2019. A real-time kinematic (RTK) survey system was used to measure ground control point (GCP) positions for georeferencing the TLS reconstructed point clouds. Embankment deformations were determined by point cloud comparison. TLS deformations were compared to instrumentation deformation data. This paper presents the methodology and results of the TLS deformation monitoring. Limitations of the technologies are discussed and recommendations for deformation monitoring using TLS are provided.

RÉSUMÉ
L'autoroute Inuvik-Tuktoyaktuk (ITH) dans les Territoires du Nord-Ouest, au Canada, a été construite pendant l'hiver sur du pergélisol continu riche en glace sans aucune entaille dans le sol pour préserver la fondation du pergélisol. Plusieurs sections à haut remplissage étaient nécessaires le long de la route pour répondre aux spécifications de géométrie verticale. Les remblais des régions arctiques sont susceptibles de se déformer en raison de la décongélation du matériau de remblayage gelé et de la fondation du pergélisol au niveau des orteils du remblai. Une section à haut remplissage le long de l'ITH a été renforcée avec des géotextiles tissés pour réduire les mouvements de pente. La section renforcée et une section de contrôle adjacente ont été instrumentées pour surveiller les mouvements des pentes. Un balayage laser terrestre (TLS) a été effectué sur le site de recherche en août 2018 et juin 2019. Un système de levé cinématique en temps réel (RTK) a été utilisé pour mesurer les positions des points de contrôle au sol (GCP) pour géoréférencer les nuages de points reconstruits TLS. Les déformations du remblai ont été déterminées par comparaison de nuages de points. Les déformations TLS ont été comparées aux données de déformation de l'instrumentation. Cet article présente la méthodologie et les résultats de la surveillance de la déformation TLS. Les limites des technologies sont discutées et des recommandations pour la surveillance de la déformation à l'aide de TLS sont fournies.

1 INTRODUCTION

Embankments in Arctic regions are usually constructed during winter to improve mobility of construction equipment on the frozen ground and minimize disturbance of permafrost by reducing heat input to the ground. Fill material is often locally available, frozen soil that contains a high ice content. Melting of this ice during warming reduces the shear strength of the embankment fill (De Guzman et al. 2018) and causes instability, which is exhibited through slope movements. This is particularly observable during the first spring following construction. Another common cause of embankment instability and deformation is gradual thawing of the foundation soil at the toes. Snow drifts that build up at the toe during winter insulate the thawed ground and can prevent it from freezing (Fortier et al. 2011). Then during summer, the thawed zone extends further beneath the embankment (Esch 1983). Large thaw zones that develop at the toe due to this cyclic process cause toe subsidence and an outward movement of the slope (McGregor et al. 2010). This can lead to longitudinal

cracking along the embankment road surface and in extreme cases, slope failures.

The Inuvik-Tuktoyaktuk Highway (ITH) in Northwest Territories, Canada was built during winter on ice-rich continuous permafrost with no cuts in the ground. Several high-fill sections were required along ITH to meet vertical geometry specifications as the highway traversed thermokarst terrain. One of the high-fill sections was reinforced with wicking geotextiles to improve slope stability by reinforcing the slope and providing a direct path to transport water out of the embankment fill as ice melts during the first spring thaw. Instrumentation was installed in the reinforced test zone and a non-reinforced control zone to measure deformations within the embankment. The instrumentation provided valuable data; however, measurements were only made at a few discrete locations. To better understand the performance of the entire embankment, terrestrial laser scanning (TLS) was performed in 2018 and 2019 to monitor its deformations.

TLS is a ground-based remote sensing technology that utilizes electromagnetic radiation to acquire information of the surrounding physical environment (Abellán et al. 2014). Laser light is emitted in a single direction with a well-defined wavelength and amplitude, and distances to objects are measured based on properties of the reflected laser. Modern laser scanners emit infrared lasers and can detect extremely small energy reflections from distant surfaces. TLS has revolutionized the earth surveying and monitoring fields due to the technology's accuracy, resolution, and convenience. The combination of millimetre-level accuracy and high spatial resolution allows for detailed monitoring and a rapid increase in understanding the performance of structures. Monitoring deformations of the ITH embankment using TLS provided the opportunity to better understand the mechanisms influencing deformations of embankments in permafrost regions. This is important for predicting how these embankments will perform in the future, especially considering the significant impact climate change is having on the Arctic environment.

2 METHODS

This section details the equipment used to monitor the ITH embankment, the calibration tests performed to quantify the TLS system accuracy, the design of the TLS surveys, and the on-site data acquisition methods.

2.1 Equipment

A tripod-mounted, high-speed terrestrial laser scanner was used in this research to generate detailed 3D models of the ITH embankment. The scanner emits an infrared laser beam that is reflected off a rotating mirror towards the area being scanned and calculates distances and orientations of objects to the scanner by measuring the phase shift of the reflected beam (FARO Technologies Inc. 2015). The scanner has a distance range of 330 m and can capture data in a 360° horizontal range and 300° vertical range, only missing data directly beneath the scanner's tripod. The scanner also has a high-quality 70 Mp camera to capture imagery of the scene, allowing for full-colour 3D point clouds to be generated. The scanner was set to acquire data at a resolution of ¼ and quality of 4x, corresponding to 11 minute scans with approximately 44 million points.

Most TLS monitoring projects require several scans from a variety of positions in order to provide good structure and details of the environment (FARO Technologies Inc. 2019). The process of transforming multiple scans to be closely aligned into one consistent project coordinate system is referred to as registration. A common and effective method of registering scans is to use targets. Targets common in different scans can be identified and used as reference points to align the scans. This research utilized two types of targets: spheres and checkerboards. Sphere targets have the unique quality of appearing identical from any orientation and can be used to register scans from all directions. The sphere targets were mounted on tripods (Figure 1a) and set up throughout the survey area. Scans are registered using checkerboard targets by aligning the checkerboard centres. Checkerboard targets (Figure 1b) were prepared by cutting hardwood sheaths into 60 cm x 60 cm pieces and spray painting them black and bright pink/orange. Checkerboard targets needed to be set up vertically during scans. Thus, checkerboard stands (Figure 1c) were built for this purpose. The stands were sturdy enough to be unaffected by wind, as well as collapsible, easy to assemble, and lightweight for practicality on-site and while transporting.

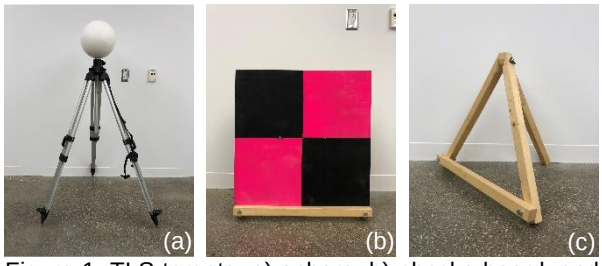

Figure 1. TLS targets: a) sphere; b) checkerboard; and c) checkerboard stand.

In order to compare TLS point clouds from different epochs, point clouds need to be georeferenced to a common coordinate system. The scanner's internal Global Navigation Satellite System (GNSS) sensor was not accurate enough on its own; therefore, a real-time kinematic (RTK) survey system was used to measure positions of checkerboard targets during scans. Checkerboard targets functioned as ground control points (GCPs) for georeferencing the reconstructed point clouds from each year to a common coordinate system.

2.2 TLS Calibration Tests and Survey Design

Several calibration tests were completed to assess the accuracy and expected errors of the TLS system,

determine optimal survey parameters, and design on-site surveys that were suitable for the site conditions. The first calibration test assessed the accuracy of the TLS system for measuring displacement of sphere targets. Six spheres were set up and four scans were performed: two with the initial sphere setup and two after sphere displacement. Spheres were displaced both vertically and horizontally, and the displacements were measured by hand. After the scans were processed, the displacement of each sphere was measured directly in the processing software and compared to the hand-measured displacements. The difference between the TLS-measured and hand-measured displacements was considered error, and the three-dimensional (3D) root mean squared (RMS) error was calculated using the following equation:

$$RMS\ error = \sqrt{\frac{\sum_{i=1}^{n} \Delta^2}{n}} \quad [1]$$

where Δ is the target error and *n* is the number of targets included in the calculation. The analysis showed that the target displacement RMS error was less than 5 mm, or only 2.8 mm if an outlier was omitted. This calibration test exhibited the TLS system's ability to measure fine displacements.

Proper setup of checkerboard targets is essential for registration and georeferencing. The viewing angle between the scanner and checkerboard target influences the number of scan points on the target and therefore the accuracy of the marked checkerboard centre. The second calibration test (Figure 2) investigated the effect of the checkerboard's standing angle (i.e. checkerboard to the ground surface) and viewing angle (i.e. checkerboard to the scanner) on the scanner's ability to accurately mark the checkerboard centre. The test included two scans from different locations, three vertical checkerboards at various viewing angles between the scans, and five checkerboards with a range of standing angles placed 25 m away from the scans. The test setup was designed based on the dimensions of the ITH embankment and estimated distances between scanners and targets on-site.

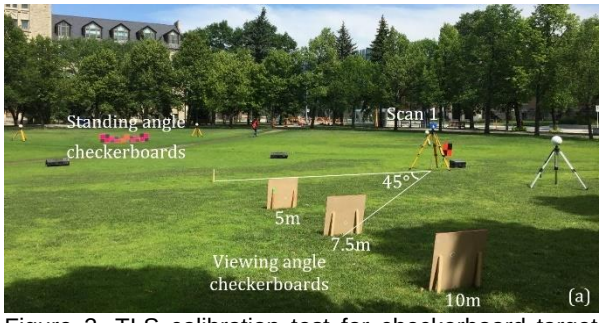

Figure 2. TLS calibration test for checkerboard target setup angles.

The calibration test results confirmed that the distances and orientations between scanners and targets was sufficient for identifying and marking the checkerboard targets. The viewing angle target at 10 m (56.3°) produced the highest density of scan points on the target. There was a moderate difference in scan point density between viewing angle targets at 10 m (56.3°) and 7.5 m (45°), but a more significant reduction in scan point density for the target at 5 m (36.9°). This observation reinforces the general guideline to limit the scanner-to-target viewing angle to a minimum of 45° (Lato 2018). As expected for the standing angle checkerboards, the vertical targets had the most scan points on their surface.

The third TLS calibration was designed to test the scanner's ability to identify targets and register scans for a survey similar to one that would be conducted on-site. The test was conducted next to a 5 m high road embankment (Figure 3). Five scans were performed with the sphere and checkerboard targets set up at the distances and angles planned for the on-site surveys. Although not all targets were able to be marked during processing, there were enough targets for accurate registration of all scans. Therefore, the survey setup was deemed acceptable and used as a reference to determine the final design of the on-site surveys.


Figure 3. TLS calibration test for site-scale survey.

2.3 On-site Data Acquisition

Two site visits were completed in August 2018 and June 2019 to acquire TLS data for deformation monitoring of the ITH embankment. The research site at KM-82 was a 6 m high, 40 m long embankment section with a toe berm on the east slope to improve stability of the sideslope. Geotextile reinforcement was installed on both sideslopes of a 20 m long section. The reinforced zone and a non-reinforced control zone were both instrumented with SAAs to measure horizontal and vertical deformations within and beneath the embankment.

The TLS surveys performed at KM-82 are summarized in Table 1 and the survey designs are shown in Figure 4. Five scans were used to survey each sideslope in both years—three along the toe and two at the shoulder. The scanner was set up at 15 m spacing parallel to the road. This provided 100% coverage of the embankment within a 45° viewing angle of the scanner and ensured a dense point cloud without occlusions. The 2018 scans used three sphere targets and nine

checkerboards for each slope, with an RTK observation times of 30 seconds at checkerboard centres. Checkerboards at ground surface were set up on the stands at a 75° standing angle to optimize the viewable surface area for scans completed along the embankment toe and shoulder. Checkerboards on the shoulder were set up vertical. Since none of the targets remained in the same position for scans of both slopes, the two slopes could not be registered together and two point clouds were generated. In 2019, six spheres and ten checkerboards were used on each slope, and the RTK observation time was increased to 60 seconds at each checkerboard to reduce positional measurement errors. Additionally, six targets (two spheres and four checkerboards) that were set up along the road surface remained in position and were scanned for both slopes (Figure 4). This allowed the entire embankment to be registered into one point cloud. Figure 5 shows the TLS survey setup at the west slope in 2019.

Table 1. TLS data acquisition summary.

Year	Slope	No. scans	No. spheres	No. checker-boards	RTK time (sec)
2018	East	5	3	9	30
	West	5	3	9	30
2019	East	5	6	10	60
	West	5	6	10	60

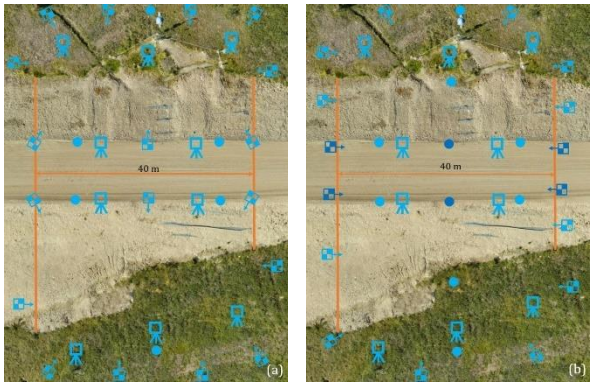

Figure 4. TLS survey plans with scanner and target locations: a) 2018; and b) 2019. Dark blue targets in 2019 remained for scans of both slopes.

3 DATA ANALYSIS

This section outlines the methods used to process the TLS data, align the 2018 and 2019 point clouds, and measure deformation of the high-fill embankment.


Figure 5. 2019 TLS survey at the research embankment west slope.

3.1 Data Processing

The following approach was used for processing TLS data from 2018 and 2019. First, raw scan data was imported to the processing software and preprocessed to allow for visualization of the scans and identification of targets. Two methods were used to register the scans together: target-based (TB) registration and cloud-to-cloud (C2C) registration. During TB registration, point cloud geometry was determined by identifying matching targets in different scans (i.e. correspondences) and minimizing the overall error between correspondences. GCP position data can be used with TB registration to georeference the point cloud. The scan point errors, which are the differences in point cloud positions between scans, can also be outputted from a TB registration. To define the scan point errors, two metrics are used: mean error and percentage of points with errors less than 4 mm.

Initial TB registrations produced point clouds with large errors; scan point mean errors ranged from 10 to 12 mm. These were significantly larger than the reported millimetre-scale accuracy of TLS systems (Abellán et al. 2014, FARO Technologies Inc. 2015). C2C registration was therefore implemented for fine registration. C2C registration uses the actual scan point data to align scans. C2C registrations produced point clouds with scan point errors of approximately 5 mm (Table 2)—a major improvement from TB registration. A limitation of C2C registration was that the point cloud was not georeferenced because no GCPs were referenced. To address this, the point cloud was ‘locked’ after C2C registration to preserve its geometry, and TB registration was performed to georeference the locked point cloud. Several iterations of TB registration were performed to determine the optimal combination of targets to minimize georeferencing errors. The target and scan point errors of the final point clouds (Table 2) demonstrate that the TLS system and survey setup was capable of generating high-accuracy point clouds, and it was the low-accuracy GCP measurements by the RTK system that caused the relatively large georeferencing errors. The final point

clouds of each TLS survey were then exported from the processing software for further analysis.

Table 2. TLS point cloud registration errors.

Survey	Scan point errors		Target errors		
	Mean (mm)	< 4 mm (%)	Mean (mm)	SD (mm)	RMS (mm)
2018 East	4.1	50.0	15.7	6.0	16.7
2018 West	3.0	62.7	13.6	7.1	15.3
2019	5.2	41.6	16.6	6.5	17.8

3.2 Deformation Measurement

TLS-derived point clouds were compared using Multiscale Model-to-Model Cloud Comparison (M3C2; Lague et al. 2013). M3C2 has been shown to provide lower error measurements and more accurately measure small-scale deformations compared to other cloud comparison methods (Barnhart and Crosby 2013, Lague et al. 2013, Gómez-Gutiérrez et al. 2014, Stumpf et al. 2015). The method operates directly on point clouds without meshing or gridding, computes deformation along the normal surface direction, and estimates a level of detection (LoD) for each distance measurement based on local point cloud roughness and registration error. The algorithm can also be performed on a sub-sampled version of the point cloud, referred to as core points, to reduce computation time. The LoD defines the minimum statistically significant deformation that can be detected. Deformations less than the LoD are considered error or noise and those greater are considered actual deformation. Using M3C2, a spatially variable LoD is calculated for each core point using the following equation:

$$LoD = \pm 1.96\left(\sqrt{\frac{{\sigma_{d1}}^2}{n_1} + \frac{{\sigma_{d2}}^2}{n_2}} + reg\right) \quad [2]$$

where σ_d is the local roughness of each point cloud surrounding the core point, n is the number of points in each point cloud used to calculate the local roughness, *reg* is the point cloud registration error (discussed below), and ±1.96 is the normal distribution z-value for the 95% confidence interval.

The main parameters required for M3C2 comparisons are core point spacing (*s*), normal scale diameter (*D*), projection scale diameter (*d*), and *reg*. Lague et al. (2013) provided guidance on parameter selection. Trial M3C2 comparisons and a parametric study were performed to investigate the effects of changing *s*, *D*, and *d*, and determine their optimal values. *reg* was determined by calculating the combined RMS error of the GCP georeferencing errors for the point clouds being compared (Table 2). *reg* was assumed isotropic and spatially uniform.

Table 3 shows the optimal M3C2 parameters used.

Table 3. M3C2 parameters.

Normal scale *D* (m)	Projection scale *d* (m)	Core point spacing *s* (m)	Registration error *reg* (m)
Most planar: [0.5–1.0]	0.2	0.025	0.017

3.3 Point Cloud Alignment

Initial M3C2 comparisons showed an unexpected vertical difference of approximately 0.35 m between the 2018 and 2019 point clouds. Analysis of the data and discussion with the research team revealed the vertical difference was due to inconsistent measurement of the RTK base station's height above the benchmark. In 2019, the base station height was measured from the sensor to the top of a steel rod benchmark; but in 2018, the height was measured from the sensor to the ground surface beside the benchmark. The vertical difference in the RTK survey was transferred to the georeferenced point clouds and manifested as an apparent decrease in elevation when the point clouds were compared.

The solution implemented was to shift the 2019 point cloud vertically to match the elevation of the 2018 point cloud. Vertical M3C2 comparisons were performed and vertical distances between the point clouds were analyzed to determine the optimal shift distance (Table 4). Separate analyses were performed on the east and west slopes because each had its own point cloud in 2018.

Table 4. Vertical point cloud comparison results and selected vertical shifts.

Slope	Measured vertical distance distribution			Selected shift (m)
	Mean (m)	Median (m)	Peak (m)	
East	-0.340	-0.346	-0.353	+0.353
West	-0.322	-0.322	-0.316/-0.337*	+0.322

* vertical distance distribution resembled a bimodal distribution with two peaks.

After the vertical shift was applied, M3C2 comparisons were performed again. The comparisons identified that there was positive change (e.g. soil deposition, heave, etc.) on the west slope and negative change (e.g. erosion, settlement, etc.) on the east slope. However, such extreme differences between the east and west slopes did not seem realistic and there was no reasonable explanation for the west slope to be heaving while the east slope was settling. Embankment deformations were expected to be more uniform on both slopes than these comparisons detected. Additionally, variability of the measured vertical difference between the 2018 and 2019 point clouds (Table 4) suggest tilting was present in at least one of the point clouds.

The authors' hypothesis is that during one or some of the RTK surveys of GCPs, the RTK base station was not levelled correctly. This tilt in the base station was transferred to the GCP measurement and subsequently to the TLS point clouds, manifesting as non-uniform—positive and negative—slope deformations (Figure 6). To correct the tilting, the 2018 and 2019 point clouds were aligned using the iterative closest point (ICP) algorithm. ICP is an iterative least squares matching algorithm that aligns two point clouds by minimizing the total distance between the point clouds. The point cloud being aligned was allowed to translate vertically and rotate on all three axes because the exact orientation of the tilt was unknown. Final M3C2 comparisons to determine embankment deformations were performed on the vertically shifted and fully aligned (with rotation) point clouds.

Figure 6. TLS point cloud tilting schematic.

4 RESULTS

The vertically shifted point cloud comparison (Figure 7) showed positive change (red) deformations at the upper-slope of both sideslopes. At the lower-slope, the west slope (facing northwest) showed positive change, which could have been lateral spreading, and the east slope (facing southeast) showed negative change (blue), which appeared to be toe subsidence. The non-uniform behaviour on the slopes and relatively large positive change at the upper-slopes did not seem realistic, though. These observations led to the rotation alignment of the point clouds, as discussed.

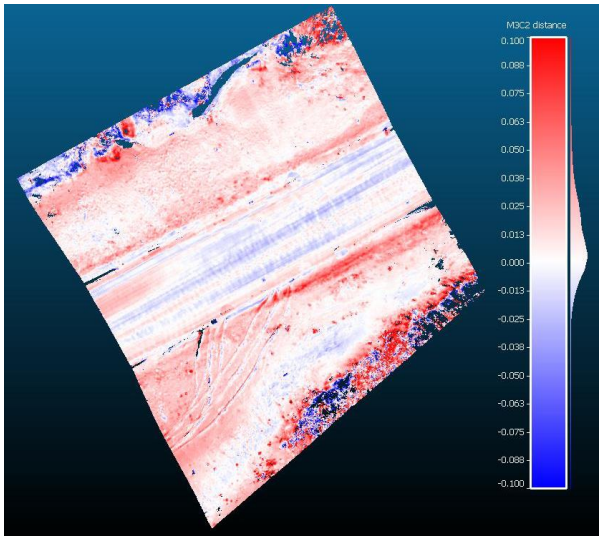

Figure 7. TLS M3C2 deformation after vertical shift (scale: ±100 mm).

The fully aligned point cloud comparison (Figure 8) produced markedly different deformations. The comparison showed negative change along the road surface, likely due to road traffic. Positive change was detected along the shoulders of the embankment, which was likely caused by spreading of the resurfacing gravel that was laid in 2017. The positive change at the upper-slope transitioned to negative change near the mid-slope and lower-slope. An explanation for the negative change would be settlement or subsidence of the slope and toe due to permafrost thawing. The TLS deformations after rotation alignment (Figure 8) were relatively uniform on both slopes and can be more reasonably explained through the lens of permafrost dynamics compared to the vertically shifted TLS deformations (Figure 7). Yet, it is difficult to conclude with confidence that the detected TLS deformations are accurate because of the point cloud modifications (e.g. vertical shift and rotation) that were applied. Mistakes made with the RTK system during data acquisition on-site necessitated the point cloud modifications to align the them for comparison; however, the alignment process majorly impacted the behaviour and magnitude of deformations that were detected. This is an important limitation of this research.

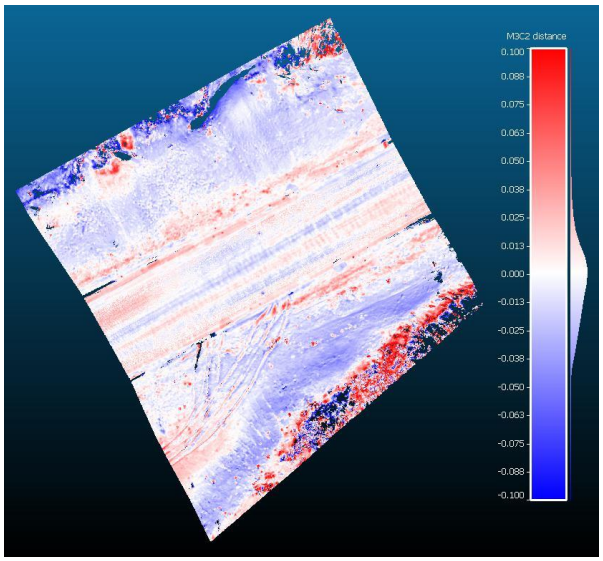

Figure 8. TLS M3C2 deformation after rotation alignment (scale: ±100 mm).

It is important to consider the deformation uncertainty estimates (i.e. LoD) and significant change outputs of the M3C2 comparisons. LoD estimates for the M3C2 comparisons (Figure 9) were 33–40 mm on the embankment. LoD estimates were higher along the toes (~45 mm) due to vegetation. The significant change estimates for the M3C2 comparisons (Figure 10) show that almost the entire embankment can not be considered actual change—red points represent significant change where deformation is greater than the LoD. If surface roughness was ignored and only registration error (*reg*) was considered for calculating

LoD (Equation 1), LoD for the TLS comparisons would be 33 mm. Comparing this value to the computed LoDs demonstrates the large influence of *reg*. Surface roughness of the embankment only contributed a maximum of roughly 5 mm to the LoD. The large *reg* values and inconclusive significant change results were due to the high GCP position errors from the RTK survey.

The poor quality of GCP data acquired on-site led to several challenges during processing and ultimately, low confidence in the final deformation results. TLS data acquired with the scanner was good, but it was the GCP data acquired with the RTK system that caused the issues and inaccuracies. Modifications of the point cloud data and high LoDs, both of which were due to poor RTK accuracy, restricted meaningful conclusions being drawn from the deformation results.

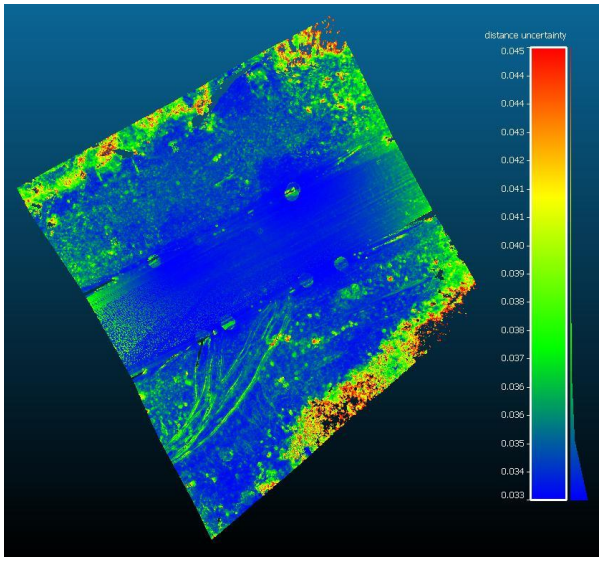

Figure 9. TLS M3C2 LoD estimates (scale: 33–45 mm).

Instrumentation in the embankment measured approximately 15 mm of vertical and lateral deformations between the 2018 and 2019 TLS surveys. The TLS deformations after full alignment with rotation were reasonably close to the instrumentation deformations. This provided some confidence that the TLS deformations could be representative of actual deformations, despite the data modifications and non-significant change estimates.

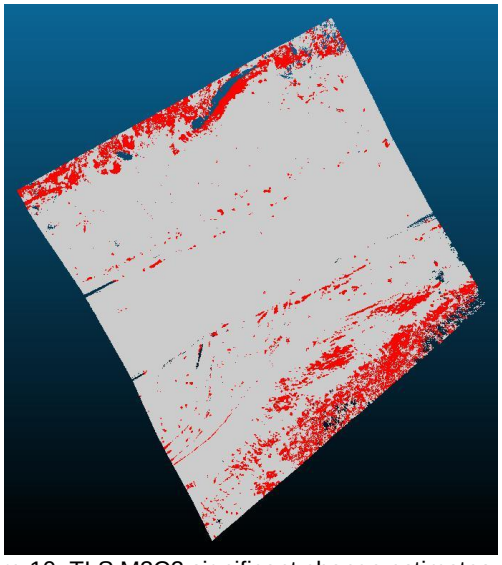
Figure 10. TLS M3C2 significant change estimates.

5 CONCLUSION

Terrestrial laser scanning (TLS) was used to monitor deformation of a 6 m high-fill embankment section along the Inuvik-Tuktoyaktuk Highway (ITH). The embankment was reinforced with geotextiles for slope stability and instrumented to measure deformations. Sphere and checkerboard targets were used to register scans, and a real-time kinematic (RTK) survey system was used to accurately measure checkerboard positions for georeferencing the TLS point clouds. Calibration tests and accuracy assessments prior to site visits suggested that the TLS system and survey setup were sufficient for detecting deformations of the ITH embankment. Due to issues with the RTK system, point clouds were not consistently georeferenced and required alignment prior to deformation measurement. Annual embankment deformation between the 2018 and 2019 point clouds was determined using the Multiscale Model-to-Model Cloud Comparison (M3C2) algorithm.

TLS surveys of the high-fill embankment showed deformations including toe subsidence, upper-slope spreading, and road surface traffic erosion. However, there is only a moderate level of confidence in the accuracy of the detected deformations due to unreliable georeferencing and forced alignment methods. Inaccurate GCP measurements by the RTK system limited the accuracy of the TLS point clouds and restricted the measurement of small-scale deformations. The TLS deformations after the final alignment with rotation were comparable to the instrumentation deformation measurements, suggesting the final alignment was reasonably accurate and the TLS deformations were representative of actual deformations. No significant differences were detected between deformations of the geotextile reinforced and non-reinforced zones.

One critical finding of this research was the importance of accurate GCPs. TLS can produce

extremely detailed point clouds; however, as this research showed, the ability of TLS to accurately measure deformations depends strongly on the accuracy of the GCP network and georeferencing process. Although GCPs may seem supplementary to the TLS data acquisition, the importance of accurate GCPs cannot be understated and appropriate time should be taken to set up a well-distributed GCP network and measure high-quality GCP positions with precise survey equipment. If an RTK system is to be used to measure GCP positions for small-scale deformation monitoring, RTK observation times need to be sufficiently high (minimum 3–5 minutes) in order to reduce measurement uncertainty. Otherwise, another surveying technique should be used to acquire GCP positions, such as a total station. A total station was not used in this research because the limitations of measuring GCPs with an RTK system were not realized early enough in the research.

6 ACKNOWLEDGEMENTS

This research work was funded by the Government of Northwest Territories Department of Infrastructure (GNWT-DOI), Transport Canada, and the Natural Sciences and Engineering Research Council of Canada (NSERC). The authors would like to acknowledge the GNWT-DOI field engineers for their on-site coordination and logistical assistance. The authors thank Kerry Lynch, geotechnical technician at the University of Manitoba, for his assistance preparing for site visits.

7 REFERENCES

Abellán, A., Oppikofer, T., Jaboyedoff, M., Rosser, N.J., Lim, M., and Lato, M.J. 2014. Terrestrial laser scanning of rock slope instabilities. Earth Surface Processes and Landforms, **39**(1): 80–97. doi:10.1002/esp.3493.

Barnhart, T.B., and Crosby, B.T. 2013. Comparing two methods of surface change detection on an evolving thermokarst using high-temporal-frequency terrestrial laser scanning, Selawik River, Alaska. Remote Sensing, **5**(6): 2813–2837. doi:10.3390/rs5062813.

Esch, D.C. 1983. Design and Performance of Road and Railway Embankments on Permafrost. *In* 4th International Conference on Permafrost.

FARO Technologies Inc. 2015. FARO Laser Scanner Focus3D X 330 Manual.

FARO Technologies Inc. 2019. Laser Scanner Best Practices.

Fortier, R., LeBlanc, A.-M., and Yu, W. 2011. Impacts of permafrost degradation on a road embankment at Umiujaq in Nunavik (Quebec), Canada. Canadian Geotechnical Journal, **48**: 720–740. doi:10.1139/T10-101.

Gómez-Gutiérrez, Á., de Sanjosé-Blasco, J.J., de Matías-Bejarano, J., and Berenguer-Sempere, F. 2014. Comparing two photo-reconstruction methods to produce high density point clouds and DEMs in the Corral del Veleta Rock Glacier (Sierra Nevada, Spain). Remote Sensing, **6**(6): 5407–5427. doi:10.3390/rs6065407.

De Guzman, E.M.B., Stafford, D., Alfaro, M.C., Doré, G., and Arenson, L.U. 2018. Large-scale direct shear testing of compacted frozen soil under freezing and thawing conditions. Cold Regions Science and Technology, **151**: 138–147. doi:10.1016/j.coldregions.2018.03.011.

Lague, D., Brodu, N., and Leroux, J. 2013. Accurate 3D comparison of complex topography with terrestrial laser scanner: Application to the Rangitikei canyon (N-Z). ISPRS Journal of Photogrammetry and Remote Sensing, **82**: 10–26. International Society for Photogrammetry and Remote Sensing, Inc. (ISPRS). doi:10.1016/j.isprsjprs.2013.04.009.

Lato, M. 2018. Personal communication (interview).

McGregor, R., Hayley, D., Wilkins, G., Hoeve, E., Grozic, E., Roujanski, V., Jansen, A., and Doré, G. 2010. Guidelines for Development and Management of Transportation Infrastructure in Permafrost Regions. Transportation Association of Canada. Ottawa.

Stumpf, A., Malet, J.P., Allemand, P., Pierrot-Deseilligny, M., and Skupinski, G. 2015. Ground-based multi-view photogrammetry for the monitoring of landslide deformation and erosion. Geomorphology, **231**: 130–145. Elsevier B.V. doi:10.1016/j.geomorph.2014.10.039.